PERGAMON

International Journal of Solids and Structures 38 (2001) 4901–4920

INTERNATIONAL JOURNAL OF SOLIDS and STRUCTURES

www.elsevier.com/locate/ijsolstr

Failure of sandwich beams with metallic foam cores

T.M. McCormack [a], R. Miller [b], O. Kesler [c], L.J. Gibson [c,*]

[a] *Department of Mechanical Engineering, Massachusetts Institute of Technology, Cambridge, MA 02139, USA*
[b] *Department of Mechanical Engineering, University of Saskatchewan, Saskatoon Sask., Canada S7N5A9*
[c] *Department of Materials Science and Engineering, Massachusetts Institute of Technology, 77 Massachusetts Avenue, Cambridge, MA 02139, USA*

Received 2 February 2000

Abstract

Sandwich beams with metallic foam cores can fail by several modes: face yielding, face wrinkling, core yielding and indentation. We estimate the initial failure load, corresponding to the first deviation from linearity in the load–deflection curve as well as the peak load for each mode. Failure mode maps are constructed which illustrate the dominant failure mode for practical beam designs. The results of the analysis are compared with experiments on sandwich beams with aluminum foam cores in three-point bending. The peak loads and the failure modes are described well by the analysis.

Keywords: Sandwich panels; Metal foams; Failure; Strength

1. Introduction

Sandwich beams with two stiff faces separated by a lightweight core are efficient in bending. Conventional sandwich technology uses honeycomb cores for lightweight aerospace structures and polymer foam cores for building panels. Honeycomb-core sandwiches are the lowest weight for a given structural requirement but suffer several limitations. Durability problems have been associated with water intrusion into panels. Forming complex curved shapes is difficult. And the cores themselves are highly anisotropic. Closed-cell polymer foam cores give increased thermal insulation at moderate weight but creep even at ambient temperatures. Metallic foam core sandwich structures offer a number of advantages. They can be made with integral skins, eliminating the need for adhesive bonding, allowing them to be used at higher operating temperatures. They can be readily formed into curved shapes. And the properties of the foams are nearly isotropic.

Sandwich beams can fail by several modes: face yielding, face wrinkling, core yield, indentation and delamination. Here, we estimate the initial failure load, corresponding to the first deviation from linearity in the load–deflection curve, as well as the peak load for each mode, assuming a perfect bond between the

* Corresponding author. Tel.: +1-617-253-7107; fax: +1-617-258-6275.
E-mail address: ljgibson@mit.edu (L.J. Gibson).

0020-7683/01/$ - see front matter
PII: S0020-7683(00)00327-9

faces and the core. The relatively high Young's moduli of metallic foam cores gives rise to normal stresses which are comparable to the shear stresses in the core. Here, we make use of the Deshpande and Fleck (2000) constitutive equation to estimate the initial failure load of sandwich beams by core yielding and indentation. The peak failure load is calculated using limit load analysis. Failure mode maps are constructed which illustrate the dominant failure mode for practical beam designs. The results of the analysis are compared with experiments on sandwich beams with aluminum foam cores loaded in three-point bending. The current study has been done in parallel with those of Chen et al. (2000) and Bart-Smith et al. (2000).

2. Analysis

Consider a sandwich beam of span L and width b loaded in three-point bending (Fig. 1). The faces of the sandwich have thickness t, Young's modulus E_f, Poisson's ratio, v_f and yield strength σ_{yf}. The isotropic core of the sandwich has thickness c, Young's modulus E_c, shear modulus G_c, Poisson's ratio v_c, compressive strength σ_{yc} and shear strength τ_{yc}. The deflection of the beam under a load P is given by:

$$\delta = \frac{PL^3}{48(\mathrm{EI})_{eq}} + \frac{PL}{4(\mathrm{AG})_{eq}}. \tag{1}$$

The equivalent flexural rigidity $(\mathrm{EI})_{eq}$ and the equivalent shear rigidity $(\mathrm{AG})_{eq}$ are:

$$(\mathrm{EI})_{eq} = \frac{E_f bt(c+t)^2}{2} + \frac{E_f bt^3}{6} + \frac{E_c bc^3}{12} \approx \frac{E_f btc^2}{2}. \tag{2a}$$

$$(\mathrm{AG})_{eq} = \frac{G_c b(c+t)^2}{c} \approx G_c bc. \tag{2b}$$

The approximations are valid if the faces are thin relative to the core and if the core material is compliant relative to the faces. In the case of a metallic foam core, the unloading moduli are higher than the loading moduli due to local plasticity observed with both surface strain mapping and with computed tomography (Bart-Smith et al., 1998; Bastawros et al., 1998). The unloading moduli are used to calculate the unloading stiffness of the beam while the loading moduli are used to calculate the loading stiffness of the beam. The loading modulus, which averages the effect of the local plasticity, is used where relevant to compute failure loads.

Failure can occur by one of several modes: (i) plastic yielding of the faces (ii) wrinkling (or local buckling) of the compressive face (iii) plastic yielding of the core and (iv) indentation of the loading point

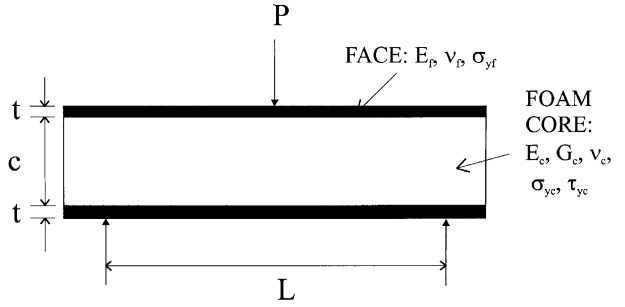

Fig. 1. Sandwich beam loaded in three-point bending.

and face sheet into the core (Fig. 2). We assume a perfect bond between the face and core so that delamination is avoided. For each failure mechanism we write an expression for the load at which failure initiates P_{in}. For the failure mechanisms involving plasticity, we also write expressions for the limit load P_{lim}. The limit load analysis for core yield and indentation follows that given in Ashby et al. (2000, Chapter 10).

2.1. Face yielding

The faces begin to yield when the maximum normal stress in the face reaches the yield stress of the face material, or when (Allen, 1969):

$$\sigma_{yf} = \frac{M\left(\frac{c}{2}+t\right)E_f}{(EI)_{eq}} \tag{3}$$

or

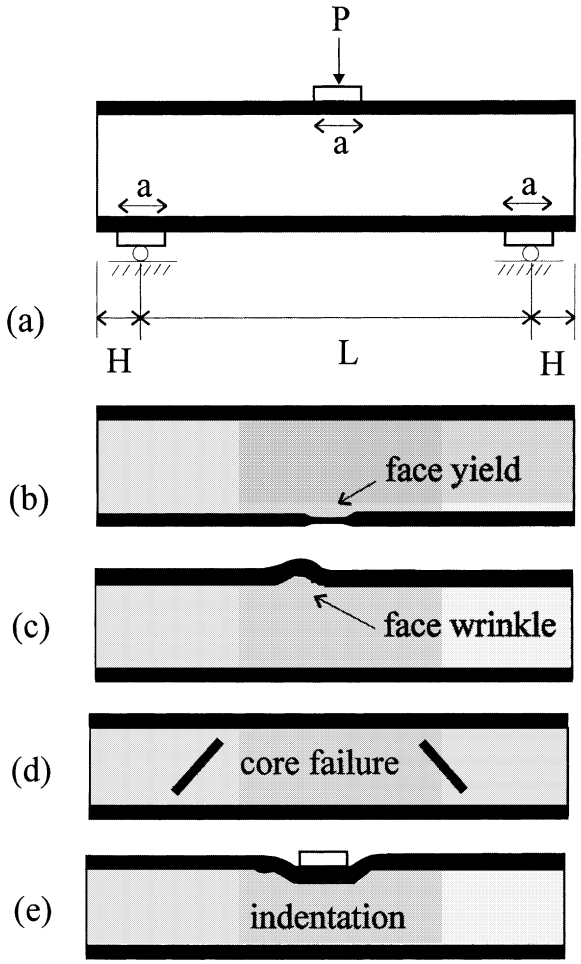

Fig. 2. Failure modes of sandwich beams: (a) loading configuration, (b) face yielding, (c) face wrinkling, (d) core yielding and (e) indentation.

$$P_{\text{in fy}} = \frac{2\sigma_{\text{yf}} btc^2}{L\left(\frac{c}{2}+t\right)}. \tag{4}$$

The limit load for face yielding is calculated by equating the applied moment to the plastic moment of the sandwich beam:

$$P_{\text{lim fy}} = 4\frac{\sigma_{\text{yf}} bt(c+t)}{L}. \tag{5}$$

For faces that are thin compared to the core, the load for the initiation of failure is approximately equal to the limit load.

2.2. Face wrinkling

The compressive face wrinkles when the normal stress reaches the local elastic instability stress, or when (Allen, 1969):

$$P_{\text{fw}} = 2.28E_{\text{f}}^{1/3}E_{\text{c}}^{2/3}\frac{btc}{L}. \tag{6}$$

2.3. Core yield

The load at which core yielding initiates is calculated by substituting the elastic stress state into the yield surface for a metallic foam. In the elastic regime, the stress state in the core is a superposition of an approximately constant shear stress τ_{core} and a normal stress σ_{core} that increases linearly with distance from the neutral axis. The point under greatest stress is directly below the central load, at the interface between the core and face. We develop an expression for the critical value of the load $P_{\text{in cy}}$ to cause the core to begin yielding at this point. The stresses at the critical point are

$$\sigma_{\text{core}} = \frac{PL}{4btc}\frac{E_{\text{c}}}{E_{\text{f}}} \tag{7}$$

$$\tau_{\text{core}} = \frac{P}{2bc} \tag{8}$$

and thus the ratio of the shear stress to the normal stress is

$$\frac{\tau_{\text{core}}}{\sigma_{\text{core}}} = 2\frac{t}{L}\frac{E_{\text{f}}}{E_{\text{c}}}.$$

For many sandwich beams designs, this ratio is large and it is a good approximation to treat the core stress state as one of pure shear. However, for sandwich beams with aluminum foam cores like the ones considered here the stress ratio is of order unity and thus the full multiaxial stress state must be considered in the core.

Taking the direction along the length of the beam to be the X_1 direction, the stress state in the core can be written as

$$\sigma = \begin{bmatrix} \sigma_{\text{core}} & \tau_{\text{core}} & 0 \\ \tau_{\text{core}} & 0 & 0 \\ 0 & 0 & \nu'\sigma_{\text{core}} \end{bmatrix} = \frac{P}{2bc}\begin{bmatrix} A & B & 0 \\ B & 0 & 0 \\ 0 & 0 & \nu' A \end{bmatrix}, \tag{9}$$

where

$$A = \frac{E_c/E_f}{2t/L} \quad B = 1$$

and v', has been used to include both plane stress and plane strain approximations in the analysis. For plane strain (a good approximation near the center of a wide beam) $v' = v_c$, while for plane stress (a good approximation at the free surface of the core) $v' = 0$.

The yield surface of the metallic foam core is well described by (Deshpande and Fleck, 2000):

$$\frac{1}{1+\left(\frac{\beta}{3}\right)^2}\left[\left(\frac{\sigma_e}{\sigma_{yc}}\right)^2 + \beta^2\left(\frac{\sigma_m}{\sigma_{yc}}\right)^2\right] = 1, \tag{10}$$

where σ_m and σ_e are the mean and von Mises equivalent stresses, respectively and β is a constant related to the compressibility of the foam during plastic deformation. For the aluminum foam used here, previous studies have shown that $\beta = 2.045$ (Deshpande and Fleck, 2000; Gioux et al., 2000).

The load for initiation of core yield failure $P_{in\,cy}$ is found by substituting the stress state (Eq. (9)) into the yield surface (Eq. (10)) to give

$$P_{in\,cy} = 2\sigma_{yc}bc\sqrt{\frac{1+(\beta/3)^2}{A^2(1-v'+v'^2)+3B^2+\beta^2A^2\left(\frac{1+v'}{3}\right)^2}}. \tag{11}$$

At the limit load, shear loads in sandwich beams are carried primarily by the core which can fail by one of two modes (Fig. 3). In collapse mode A, core shear is accompanied by the formation of plastic hinges at the loading point. Note that the overhangs, extending to the left and right of the two support points, are also constrained to shear by compatibility with the adjacent material. In collapse mode B, core shear is accompanied by the formation of plastic hinges at the mid-span and at the support points. In this case, the overhangs are unloaded.

The collapse load for mode A can be found by equating the external work done by the force $P_{lim\,cy\,A}$ moving through a displacement Δ with the internal work done by shearing of the core of length $L + 2H$ and by the plastic hinges rotating through an angle θ, giving (Ashby et al., 2000):

$$P_{lim\,cy\,A} = \frac{2bt^2}{L}\sigma_{yf} + 2bc\tau_{yc}\left(1+\frac{2H}{L}\right). \tag{12}$$

Typically, the shear strength of the core is about 2/3 of the uniaxial strength.

A similar work calculation gives the plastic collapse load for mode B (Ashby et al., 2000):

$$P_{lim\,cy\,B} = \frac{4bt^2}{L}\sigma_{yf} + 2bc\tau_{yc}. \tag{13}$$

There is a transition from shearing mode A to mode B at an overhang length of

$$H_t = \frac{1}{2}\frac{t^2}{c}\frac{\sigma_{yf}}{\tau_{yc}}. \tag{14}$$

2.4. Indentation

The indentation strength of a foam, without a face sheet, is only slightly higher than the uniaxial compressive strength, as foams crush with little transverse expansion (measured values of the plastic Poisson's ratio are in the range 0.02–0.05) (Gioux et al., 2000; Deshpande and Fleck, 2000). During indentation of a sandwich beam, the loading point crushes the foam, bending the face sheet to accommodate

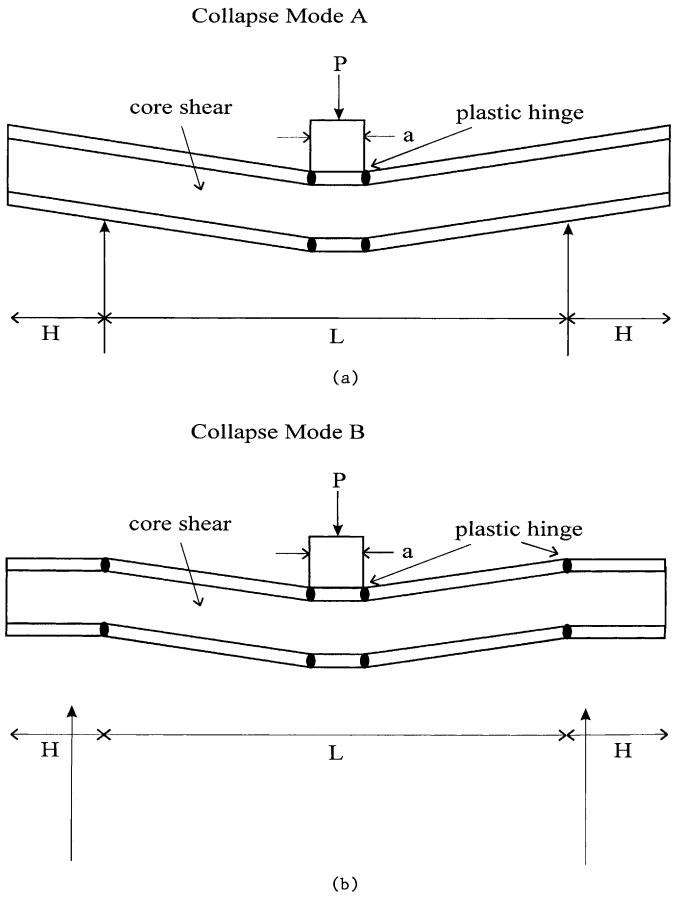

Fig. 3. Schematics of the deformed sandwich beam for core shear failure by (a) mode A and (b) mode B. (after Ashby et al., 2000, Fig. 10.4)

the foam deformation. The computation of the critical load for this to initiate is not as straightforward as the analysis of the previous mechanisms due to the complicated stress state beneath the indenter. In order to compute this load, we followed the approach of Miller (2000) who performed a series of finite element calculations of axisymmetric indentation of a sandwich beam resting on a rigid base. Here, we have repeated the finite element calculations, for the analogous plane strain model. All calculations were performed using the commercial package ABAQUS, within the finite strain formulation of incremental plasticity which is standard in this software. Elements used were a combination of 8-noded bi-quadratic plane strain quadrilaterals and 6-noded quadratic plane strain triangles. The constitutive model of the aluminum foam is elastic–perfectly plastic. The elastic behavior assumes a Poisson's ratio of 0.33 and various values of Young's modulus. The yield surface is that of Deshpande and Fleck (2000) (Eq. (10)). Densification of the foam was included by inputting a piecewise linear approximation to a typical uniaxial compression curve for a metal foam. The dense aluminum face sheets were modeled as elastic–perfectly plastic Mises material, with Poisson's ratio $\nu_f = 0.33$.

The finite element results indicate that failure takes place by localized collapse of the foam core directly beneath the indenter, with a limited plastic zone in the core on either side of the indenter (Fig. 4a). At the same time, two plastic hinges form in the face at the edges of the indenter while the face beyond the indenter

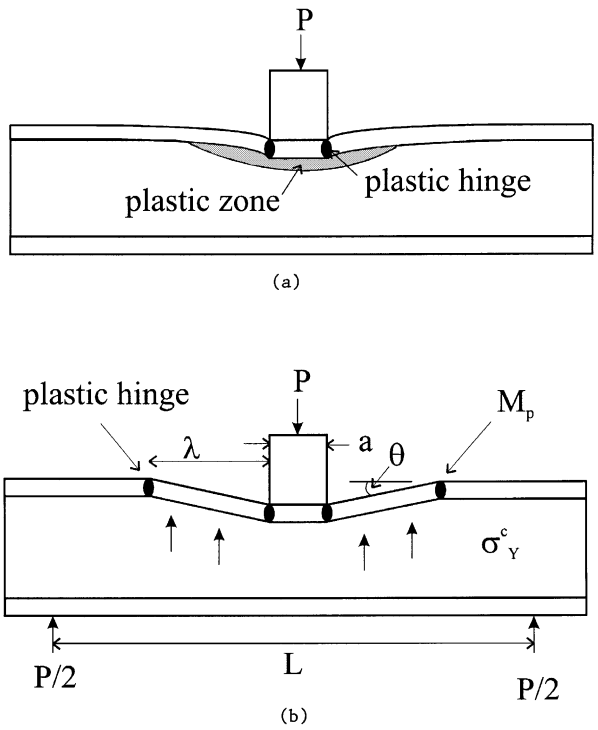

Fig. 4. Schematics of deformed sandwich beam at (a) initiation of indentation and (b) limit load for indentation (after Ashby et al., 2000, Fig. 10.3).

deforms by plate bending, as well as stretching when the indentation depths become large. The limit load for this failure mechanism can be shown to be:

$$P_{\mathrm{i}} = \sqrt{2}bt\sqrt{\sigma_{\mathrm{yf}}\sigma_{\mathrm{yc}}} + ab\sigma_{\mathrm{yc}}. \tag{15}$$

A parametric study varying the material properties and geometry of the beam and indenter indicated that, to a good approximation, indentation failure initiated at a load of

$$P_{\mathrm{in\,ind}} = 0.7\left[\sqrt{2}bt\sqrt{\sigma_{\mathrm{yf}}\sigma_{\mathrm{yc}}} + ab\sigma_{\mathrm{yc}}\right]. \tag{16}$$

We take this as an approximation of the initiation of indentation failure in a sandwich beam loaded in three-point bending.

At the limit load for three-point bending, four plastic hinges form in the face, as shown in Fig. 4b. Note that in this case, two additional plastic hinges form a distance λ away from the edges of the indenter. An upper bound for the indentation load $P_{\mathrm{lim\,in}}$ can be found by equating the plastic work done by the force $P_{\mathrm{lim\,in}}$ with that done in rotating the four plastic hinges through the angle θ (Ashby et al., 2000):

$$P_{\mathrm{lim\,in}} = \frac{4M_{\mathrm{p}}}{\lambda} + (a+\lambda)b\sigma_{\mathrm{yc}}. \tag{17}$$

Minimization of $P_{\mathrm{lim\,in}}$ with respect to λ gives

$$\lambda = t\sqrt{\frac{\sigma_{\mathrm{yf}}}{\sigma_{\mathrm{yc}}}}. \tag{18}$$

Substituting for λ gives the upper bound for the limit load for indentation

$$P_{\text{lim in}} = 2bt\sqrt{\sigma_{\text{yc}}\sigma_{\text{yf}}} + ab\sigma_{\text{yc}}. \tag{19}$$

The lower bound is calculated by considering equilibrium. It gives the same result for the indentation load as the upper bound solution (Eq. (19)) which, then, must be exact.

Eqs. (4), (6), (11) and (16) give the loads for initiation of failure by each mode while Eqs. (5), (12), (13) and (19) give the limit loads for the ultimate load carrying capacity of the beam for each mode.

The dominant mechanism, for a given design, is the one giving failure at the lowest load. A transition in failure mechanism takes place when two mechanisms have the same failure load. This information can be displayed in a failure map (Fig. 5). The axes are the design parameters of the beam, the normalized face and core thicknesses, t/L and c/L. The diagram is divided into fields, within which one failure mechanism is dominant. The fields are separated by transition lines, which represent the beam designs for which two mechanisms have the same failure load. For the aluminum foam core sandwich beams tested in this study, the dominant failure modes are indentation and core shear (modes A and B). The equation of the transition line between the indentation and mode B core shear failure is found by setting Eqs. (19) and (13) equal, giving:

$$2\sqrt{\sigma_{\text{yf}}\sigma_{\text{yc}}}\left(\frac{t}{L}\right) + 4\sigma_{\text{yf}}\left(\frac{t}{L}\right)^2 + \left(\frac{a}{L}\right)\sigma_{\text{yc}} = 2\tau_{\text{yc}}\left(\frac{c}{L}\right).$$

The equation of the transition line between the mode A and mode B core shear failure is found by setting Eqs. (12) and (13) equal, giving:

$$\frac{c}{L} = \frac{\sigma_{\text{yf}}}{\tau_{\text{yc}}}\frac{L}{2H}\left(\frac{t}{L}\right)^2$$

or a straight line with slope 2 on Fig. 5.

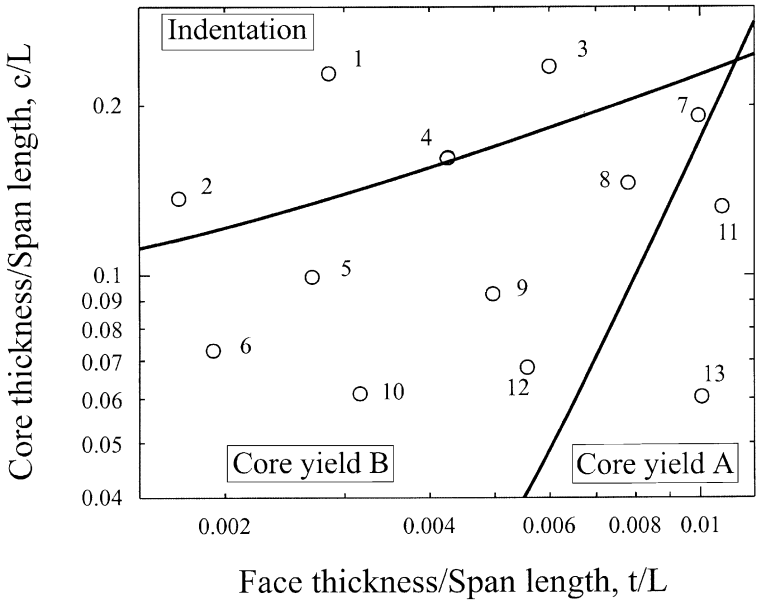

Fig. 5. Failure mode map for the limit load in three-point bending, showing designs of the sandwich beams tested.

3. Experimental methods

The faces of the sandwich beams were cut from sheets of 6061-T6 aluminum alloy. The Young's modulus and 0.2% offset yield strength of the face sheets were measured in tensile tests on dogbone specimens in an Instron testing machine. The cores of the beams were made of 8% dense aluminum foam with a cell size of approximately 4.5 mm (Alporas, Shinko Wire, Amagasaki, Japan). The properties of the aluminum foam have been measured previously (Andrews et al., 1999; Bart-Smith et al., 1998; Bastawros et al., 1998; Gioux et al., 2000); its initial yield surface is well described by the Deshpande–Fleck (2000) yield surface (Eq. (10)).

Tests on the sandwich beams, loaded in three-point bending, were designed to measure the loading and unloading stiffnesses, the load at which failure initiates (corresponding to the point at which the load–deflection curve becomes non-linear) and the limit load (corresponding to the peak load measured). A failure mode map for the failure limit load for three-point bend, with a ratio of indenter half width, a, to span, L, of 0.05, was constructed using the measured face and core properties (Table 1). For practical designs of sandwich beams, the dominant failure modes are core yielding, by modes A and B, and indentation. The ratios of the face and core thicknesses to the span of the beams were selected to test the validity of the boundaries between the failure modes on the failure map; the design ratios of t/L and c/L are shown in Fig. 5. The core thickness was always greater than about six cell diameters to avoid size effects (Onck et al., 2000; Andrews et al., 2000). The width of all beams was designed to equal the core thickness to avoid anticlastic bending. The geometries of the 13 beam designs tested are listed in Table 2.

The beams were made by adhesively bonding the faces to the foam core using a commercially available structural adhesive (FM 300, Cytec Industries, West Paterson, NJ). After cleaning the faces and foam core with solvents, the assembled panel was placed in an autoclave at 350°C and 0.14 MPa for 50 min to cure the adhesive. Sandwich beams of the desired width and span were cut from large bonded plates using a band saw. Three specimens of each design were tested.

The testing procedure followed ASTM standard C393-94 (1995). Three steel fixtures of appropriate size (length $= a$) were first attached to the specimen at the support and load points, using a quick-drying adhesive (Duco cement, Devcon, Wood Dale, IL). The specimen was then placed on a three-point bending jig mounted on an Instron loading frame (Model 4201, Instron, Canton, MA). Load was applied at a constant rate of 1.5 mm/min and measured with a 5 kN load cell. Several times prior to failure, the beam was unloaded to obtain unloading stiffness data. Deflection of the top and bottom of the midspan were measured with two LVDTs (Models 0241 and 0244, TransTek, Ellington, CT), allowing indentation to be detected. Load and deflection data were recorded on a PC using the software package LabView (National Instruments, Austin, TX) at a sampling rate of 4 Hz. The two displacements were arbitrarily offset on the

Table 1
Measured material properties of aluminum foam core and aluminum 6061-T6 alloy faces

Face	
Young's modulus, E_f	68.5 GPa
Poisson's ratio, ν_f	0.33
Yield strength, σ_{yf}	263 MPa
Core	
Loading Young's modulus, $E_{c\,loading}$	0.25 GPa
Unloading Young's modulus, $E_{c\,unloading}$	1.15 GPa
Loading shear modulus, $G_{c\,loading}$	0.096 GPa
Unloading shear modulus, $G_{c\,unloading}$	0.350 GPa
Compressive strength, σ_{yc}	1.52 MPa
Shear strength, τ_{yc}	1.00 MPa
Plastic Poisson's ratio, ν_{pl}	0.024

Table 2
Sandwich beam designs

Design #	a (mm)	L (mm)	Average H (mm)	t (mm)	c (mm)	b (mm)	t/L	c/L
1	19.5	176	11.5	0.50	40	40	0.00285	0.22792
2	31.0	292	17.1	0.50	40	40	0.00171	0.13699
3	1.55	132	9.33	0.79	31	31	0.00598	0.23485
4	19.5	185	19.7	0.79	30	30	0.00427	0.16216
5	31.0	293	22.2	0.79	29	29	0.00270	0.09898
6	45.0	410	25.7	0.79	30	30	0.00193	0.07317
7	12.5	125	16.6	1.24	24	24	0.00992	0.19200
8	15.5	158	26.1	1.24	23	23	0.00785	0.14557
9	25.0	250	35.3	1.24	23	23	0.00496	0.09200
10	40.0	392	25	1.24	24	24	0.00316	0.06122
11	19.5	182	11.2	1.96	24	24	0.01077	0.13187
12	40.0	352	21.5	1.96	24	24	0.00557	0.06818
13	40.0	397	27	3.98	24	24	0.01003	0.06045

force–displacement curves to distinguish the two measurements. A digital camera (Tm-1001-02 Pulnix, Sunnyvale, CA) recorded images of the specimen once every 30 s during the test.

The initial failure load was determined from the first deviation from linearity of the linear portion of the load–deflection curve. The mode of failure was identified from examination of the load–top deflection and load–bottom deflection curves, as well as from the series of images obtained during the test. The limit load was taken as the peak measured load.

4. Results and discussion

The dominant failure modes observed were core yielding (mode A and mode B) and indentation. Three of the 39 beams tested failed, unexpectedly, by face wrinkling. Typical load–deflection curves for each failure mode, along with sequences of images showing the progression of failure, are shown in Figs. 6–8.

The load–deflection curve for failure by core yielding (mode B) is initially linear (Fig. 6a). Three unloading cycles, of greater stiffness than the loading curve, are shown on the plot. The load increases non-linearly, corresponding to plastic yielding of the core in shear, well beyond the end of the linear regime. At the peak value a crack develops in the core and the load decreases rapidly. A large crack in the foam core, oriented at an angle of about 45°, is apparent in the images in Fig. 6d and e; the crack is a mode I tensile fracture resulting from the shear loading. The load–deflection curve for core yielding by mode A is similar to that for mode B.

The load–deflection curve for indentation failure is also initially linear (Fig. 7a). Beyond the peak load the upper LVDT trace records larger deflections than the lower LVDT, corresponding to the indentation of the top face of the sandwich. The indentation failure is clearly visible in the images of Fig. 7d and e. Plastic hinges form in the faces and there is localized crushing of the foam core beneath the indenter.

The load–deflection curve corresponding to face wrinkling failure shows a non-linear increase in load beyond the initial linear regime up to a peak load, at which point the load drops off dramatically (Fig. 8a). At the peak load, the top face can be seen to be deforming away from the core in the area adjacent to the loading pad (Fig. 8c–e). The loading pad appears to rotate as the deflection increases, suggesting that the foam beneath it may be softer on one side than the other. We speculate that the wrinkling failure is related to variability in the foam core properties, producing rotation of the loading pad and a stress concentration in the face. A thin layer of the foam core was still bonded to the face after the testing was complete, suggesting that debonding was not responsible for the wrinkling failure.

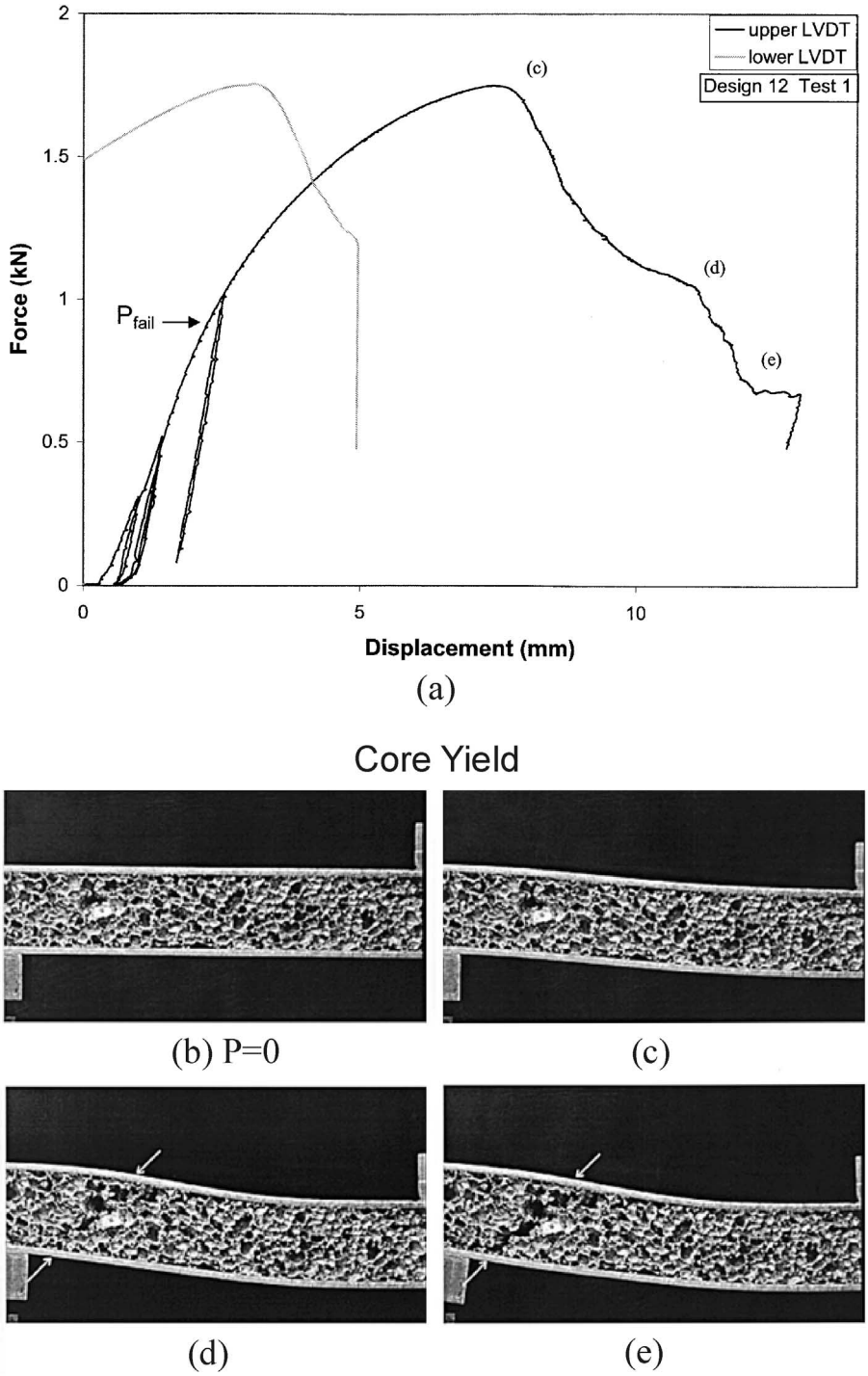

Fig. 6. (a) Load–deflection curve for a typical beam which failed by core yield (mode B) (design 12, test 1). The deflection of the top and bottom LVDTs are staggered on the plots for clarity. (b)–(e) Images of the same beam at loads corresponding to zero load and points (c)–(e) on the load–deflection curve.

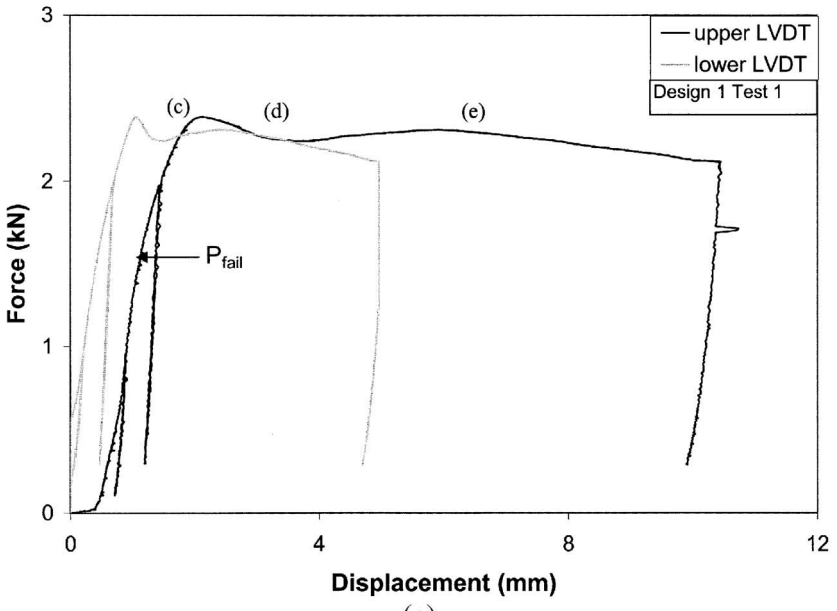

(a)

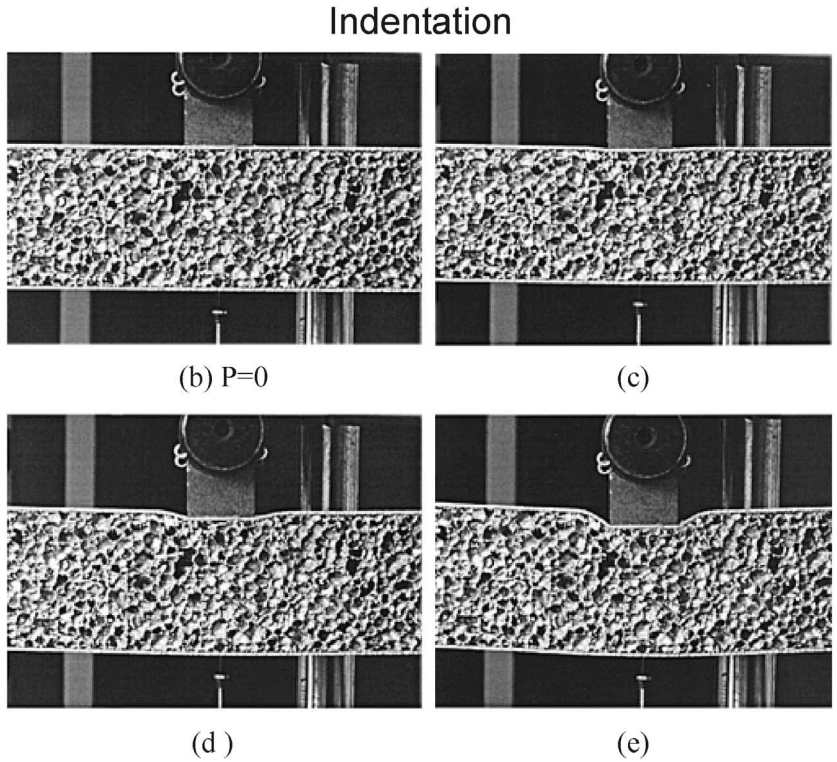

(b) P=0 (c)

(d) (e)

Fig. 7. (a) Load–deflection curve for a typical beam which failed by indentation (design 1, test 1). The deflection of the top and bottom LVDTs are staggered on the plots for clarity. (b)–(e) Images of the same beam at loads corresponding to zero load and points (c)–(e) on the load–deflection curve.

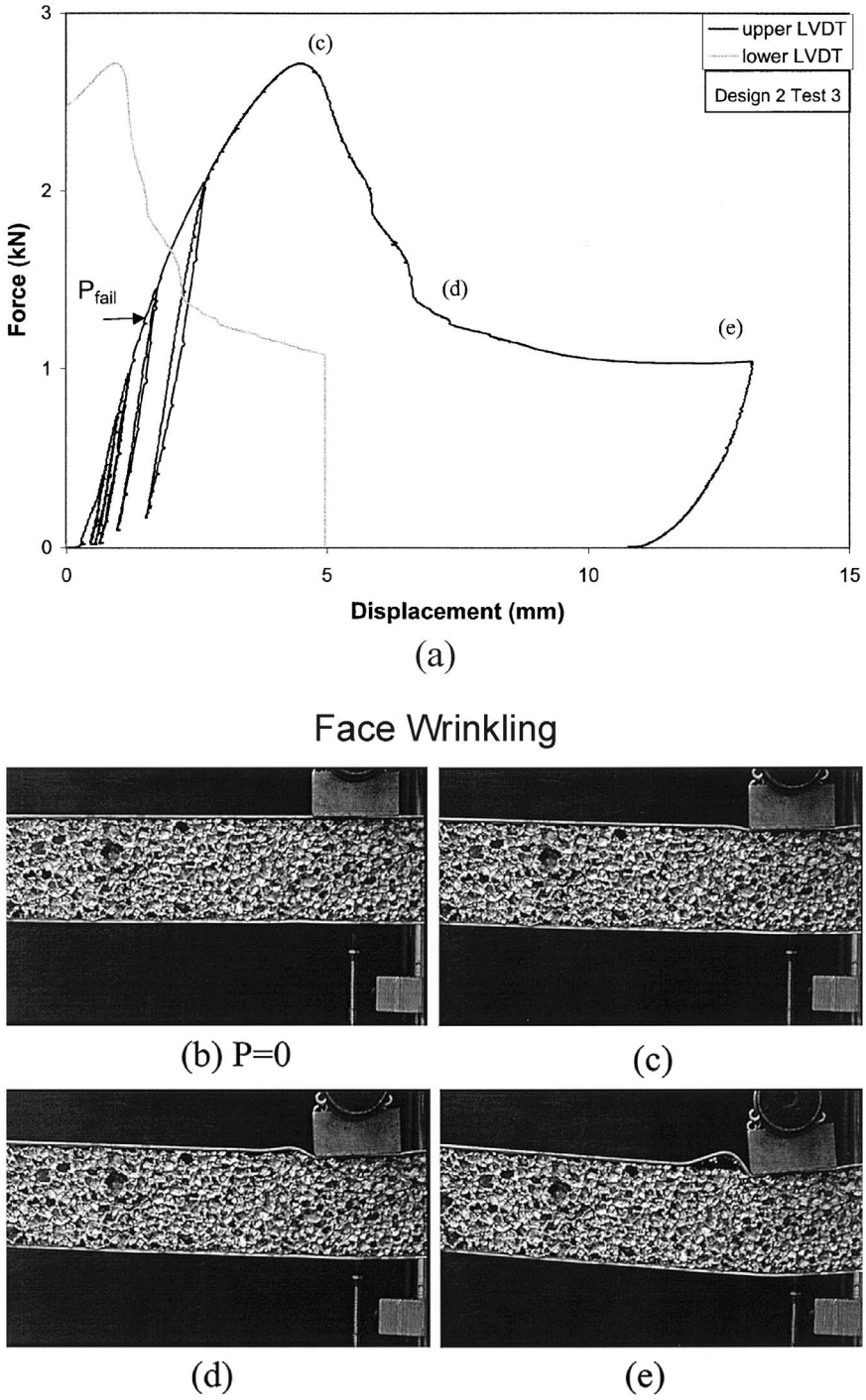

Fig. 8. (a) Load–deflection curve for a typical beam which failed by face wrinkling (design 2, test 3). The deflection of the top and bottom LVDTs: linear voltage displacement transducer are staggered on the plots for clarity. (b)–(e) Images of the same beam at loads corresponding to zero load and points (c)–(e) on the load–deflection curve.

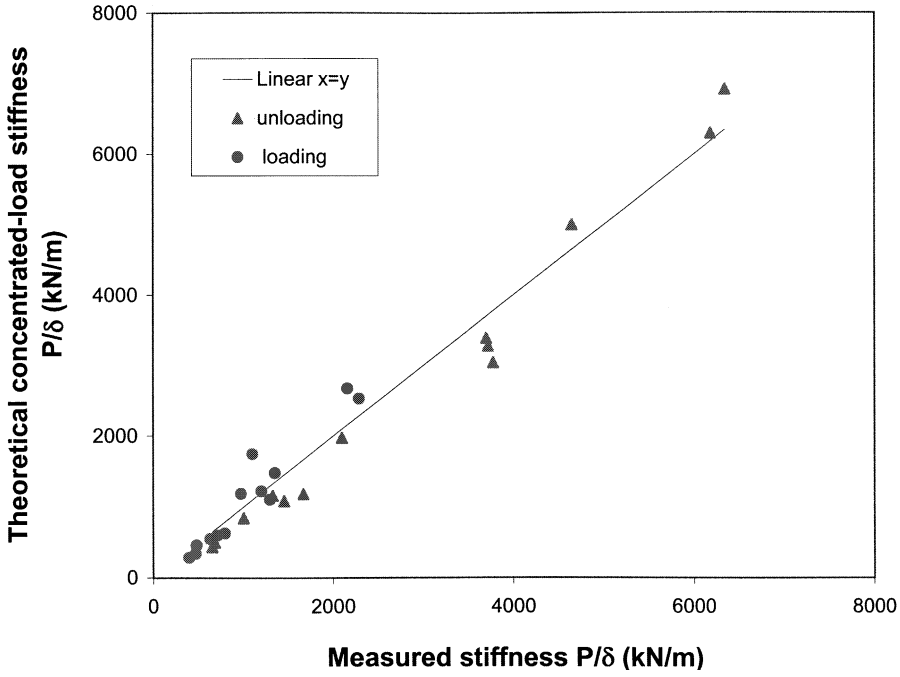

Fig. 9. Calculated beam stiffnesses plotted against measured beam stiffnesses.

The measured loading and unloading stiffnesses are compared with calculated values (Eq. (1)) in Fig. 9. The unloading stiffnesses are described well by Eq. (1). The measured loading stiffnesses were lower than the values calculated using Eq. (1) for the stiffest beams. This discrepancy may arise from the larger variability in measured values of the loading Young's modulus of the foam. The calculated stiffnesses, both for loading and unloading, assume that the load is concentrated at the loading point and at the supports. In our tests, the loads were distributed over a small area at the loading pads. The beam stiffnesses were recalculated assuming that the load was uniformly distributed over the loading pads; this led to a change in the calculated stiffness of less than 5% in all cases.

The loads at which failure initiated, corresponding to the first deviation from linearity in the load–deflection plots, are listed in Table 3, along with the calculated failure loads for each mode. The failure loads for face wrinkling (Eq. (6)) and core yielding (Eq. (11)) were calculated using the loading Young's modulus for the foam core ($E_{\mathrm{c\,loading}} = 0.25$ GPa). The initial failure loads calculated by Eqs. (11) and (16) greatly overpredict the measured loads at the first deviation from linearity for all but two of the beam designs. In deriving the equations for initial failure of the sandwich beams, the foam core was assumed to be elastic–perfectly plastic. In practice, the uniaxial compression stress-strain curve for the foam first becomes non-linear at stresses of about $1/2$ the compressive plateau stress, at which point a localized deformation band forms within the specimen (Bart-Smith et al., 1998; Bastawros et al., 1998; Andrews et al., 1999). The modes of failure at the initial deviation from linearity could not be identified directly from either the images of the deformed beams or the load-deflection plots. We note that the calculated dominant failure modes for initial deviation from linearity correspond well with the observed failure modes at the limit load, described in more detail below.

The measured peak loads are listed in Table 4, along with the calculated limit loads for each mode. The equations for the limit loads for indentation and core shearing give a good description of the average measured peak loads; in general they are within 15%. The modes of failure correspond well with those

Table 3
Failure initiation loads

Design #	P_{fy} (kN) Eq. (4)	P_{fw} (kN) Eq. (6)	P_{cy} (kN) Eq. (11)	P_{ind} (kN) Eq. (16)	Calculated initial failure load (kN) and failure mode	Observed failure loads (kN) Observed failure modes at the limit load (% difference w.r.t. exp.)			Average initial failure load (kN) of failures by predicted mode (Average % difference w.r.t. exp.)
						Test 1	Test 2	Test 3	
1	4.68	16.9	3.10	1.23	1.23 I	1.59 I (−23.1)	1.69 I (−27.3)	1.55 I (−21.1)	1.61 (−23.9)
2	2.81	10.1	2.73	1.72	1.72 I	1.18 I (44.9)	1.11 I (54.7)	1.23 FW (39.2)	1.15 (49.6)
3	5.76	21.3	2.00	0.996	0.996 I	1.25 I (−20.0)	1.21 I (−17.6)	1.49 I (−32.9)	1.31 (−24.1)
4	3.84	14.2	1.83	1.09	1.09 I	1.16 I (−5.66)	0.79 I (38.3)	0.97 I (12.6)	0.97 (12.3)
5	2.26	8.39	1.61	1.41	1.41 I	0.86 CY (64.9)	0.70 CY (102)	0.88 I (60.2)	0.88 (60.2)
6	1.73	6.42	1.59	1.91	1.59 CY	0.66 FW (143)	0.62 FW (155)	0.70 CY (128)	0.70 (128)
7	5.45	21.2	1.21	0.908	0.908 I	0.74 I/B (23.2)	0.68 I/B (32.8)	1.02 I/B (−10.9)	0.81 (11.7)
8	3.94	15.4	1.11	0.944	0.944 I	0.63 I/B (49.3)	0.52 I/B (82.9)	0.98 I/B (−3.4)	0.71 (33.2)
9	2.49	9.71	1.09	1.18	1.09 CY	0.82 CY (32.1)	0.70 CY (55.9)	0.70 CY (56.1)	0.74 (47.1)
10	1.74	6.75	1.13	1.61	1.13 CY	0.68 CY (67.6)	0.64 CY (76.8)	0.51 CY (123)	0.61 (86.3)
11	5.61	23.0	1.22	1.43	1.22 CY	1.22 CY (−0.410)	0.70 CY (73.8)	0.76 CY (60.7)	0.89 (36.3)
12	2.90	11.9	1.19	1.95	1.19 CY	0.90 CY (32.8)	0.88 CY (36.0)	0.87 CY (36.6)	0.88 (35.1)
13	4.56	21.4	1.21	2.91	1.21 CY	0.64 CY (91.1)	0.71 CY (70.0)	0.65 CY (86.2)	0.67 (82.0)

Table 4
Limit loads

Design #	P_{fy} (kN) Eq. (5)	P_{cyA} (kN) (avg) Eq. (12)	P_{cyB} (kN) Eq. (13)	P_{ind} (kN) Eq. (19)	Calculated limit load (kN) and failure mode	Observed limit loads (kN) Observed failure modes at the limit load (% Difference w.r.t. exp.)			Average limit load (kN) of failures by predicted mode (Average % difference w.r.t. exp.)
						Test 1	Test 2	Test 3	
1	5.41	3.65	3.26	1.99	1.99 I	2.39 I (−16.8)	2.50 I (−20.5)	2.27 I (−12.5)	2.39 (−16.8)
2	3.25	3.59	3.24	2.68	2.68 I	2.56 I (4.84)	2.54 I (5.70)	2.72 FW (−1.27)	2.55 (5.27)
3	6.55	2.27	2.08	1.71	1.71 I	2.50 I (−31.5)	1.69 I (0.905)	2.29 I (−25.2)	2.16 (−20.8)
4	4.37	2.24	1.91	1.84	1.84 I	2.06 I (−10.9)	2.07 I (−11.3)	1.85 I (−0.484)	1.99 (−7.79)
5	2.58	1.97	1.75	2.28	1.75 B	1.98 B (−11.9)	1.82 B (−3.90)	2.10 I (−16.8)	1.90 (−8.09)
6	1.97	2.05	1.85	3.00	1.85 B	1.91 FW (−3.09)	2.15 FW (−13.9)	1.67 B (10.4)	1.67 (10.4)
7	6.49	1.61	1.46	1.65	1.46 B	1.33 I/B (9.83)	1.13 I/B (29.2)	1.88 I/B (−22.3)	1.45 (0.96)
8	4.72	1.53	1.29	1.68	1.29 B	1.12 I/B (15.6)	1.25 I/B (3.74)	1.88 I/B (−31.3)	1.42 (−8.65)
9	2.98	1.43	1.21	2.01	1.21 B	1.36 B (−11.3)	1.35 B (−10.5)	1.49 B (−19.0)	1.40 (−13.8)
10	2.07	1.35	1.25	2.65	1.25 B	1.53 B (−18.5)	1.36 B (−8.24)	1.46 B (−14.4)	1.45 (−13.9)
11	7.17	1.56	1.68	2.59	1.56 A	1.73 A (−10.2)	1.47 A (6.27)	1.50 A (3.85)	1.57 (−0.551)
12	3.71	1.432	1.428	3.34	1.43 B	1.75 B (−18.5)	1.58 B (−9.67)	1.39 B (2.74)	1.57 (−9.3)
13	7.14	1.81	2.16	5.28	1.81 A	1.37 A (32.3)	1.36 A (33.5)	1.80 A (0.787)	1.51 (20.1)

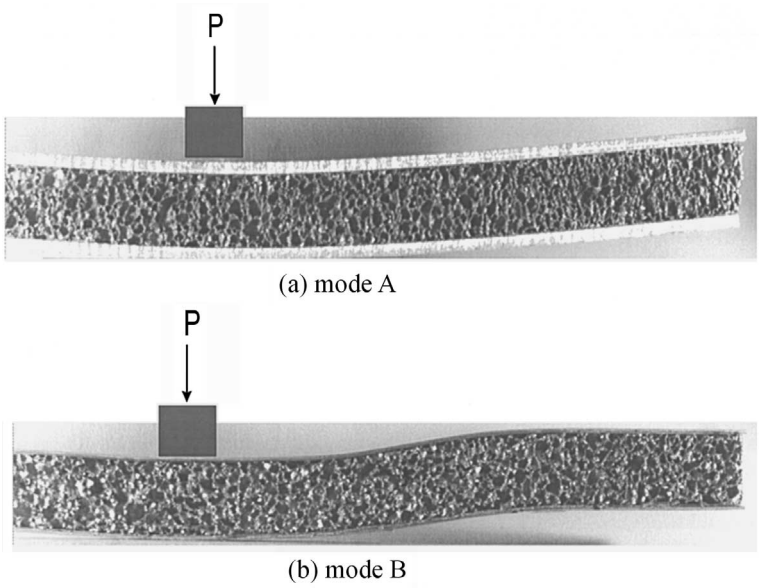

Fig. 10. Images of sandwich beams after completion of three point bend test showing core yield failure (a) mode A (design 13, test 2) and (b) mode B (design 9, test 3).

predicted by the limit loads. In beams that failed by core shearing, some failed by mode A while others failed by mode B (Fig. 10); the limit load calculation was able to distinguish these two modes of core yield failure.

For beam designs 5, 7 and 8, the calculated failure mode switches from indentation at initial failure, corresponding to the initial deviation from linearity, to core yielding by mode B at the limit load. There is evidence of both failure modes occurring in all three designs. For beam design 5, two beams were observed to fail by core yielding (mode B) while one failed by indentation. For beam designs 7 and 8, all six beams tested show evidence of both indentation and shear failure. The load–deflection curve for one of these beams, (design 8, test 2) is shown in Fig. 11a. After the peak load is reached, the curve shows both a reduction in load, associated with core shear failure, and increased deflection of the upper LVDT compared with that of the lower LVDT, indicative of indentation. An image of the beam, taken after completion of the test, shows both indentation beneath the loading point and a mode I tensile crack, resulting from the shear loading. (Fig. 11b). Note that the final indentation displacement measured on the beam (1.6 mm, Fig. 11b) roughly corresponds to the increased deflection of the upper LVDT at the completion of the test (about 2 mm, Fig. 11a). For all three beam designs (5, 7 and 8), the calculated limit loads for indentation and core yielding are close (within about 30%), compared with the differences in the limit loads for the different failure modes for the other beam designs.

Three of the beams failed, unexpectedly, by face wrinkling, possibly due to inhomogeneities in the foam beneath the loading pad. The face wrinkling failure shown in Fig. 8b–e indicates that the loading pad rotates during the loading, suggesting that the foam beneath the left side of the loading pad is less stiff than that on the right. Stress concentrations induced in the face as a result of this non-uniformity in the loading may be responsible for the face wrinkling failures. A small layer of aluminum foam remained attached to the face sheet after wrinkling occurred, suggesting that the bond between the face and the foam core did not fail. Similar behavior was observed in the other two beams that failed by face wrinkling.

The observed failure modes are compared with the failure map for the limit loads in Fig. 12. Transition lines between indentation failure and mode B core shear failure and between mode B and mode A core

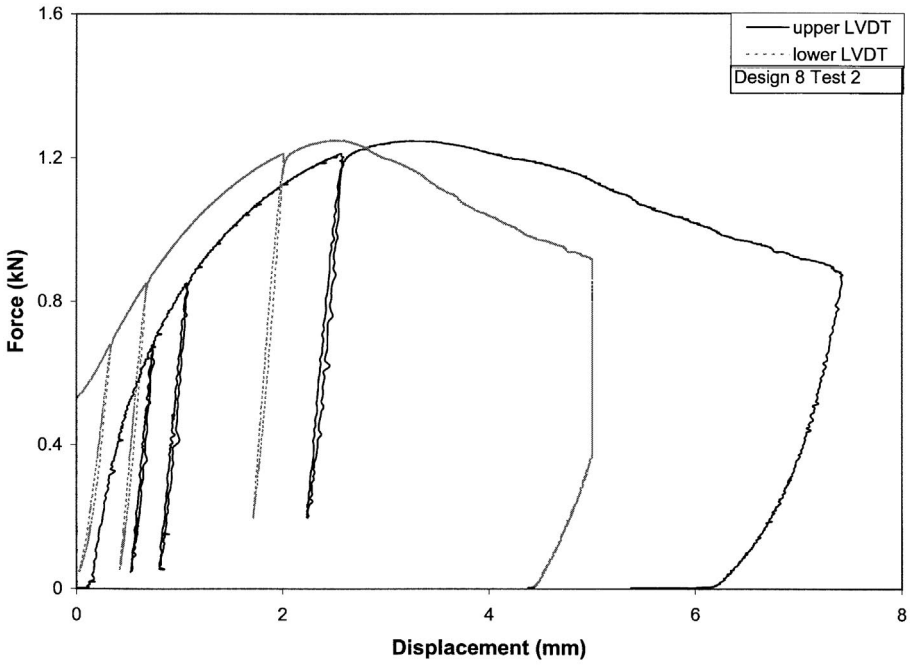

(a)

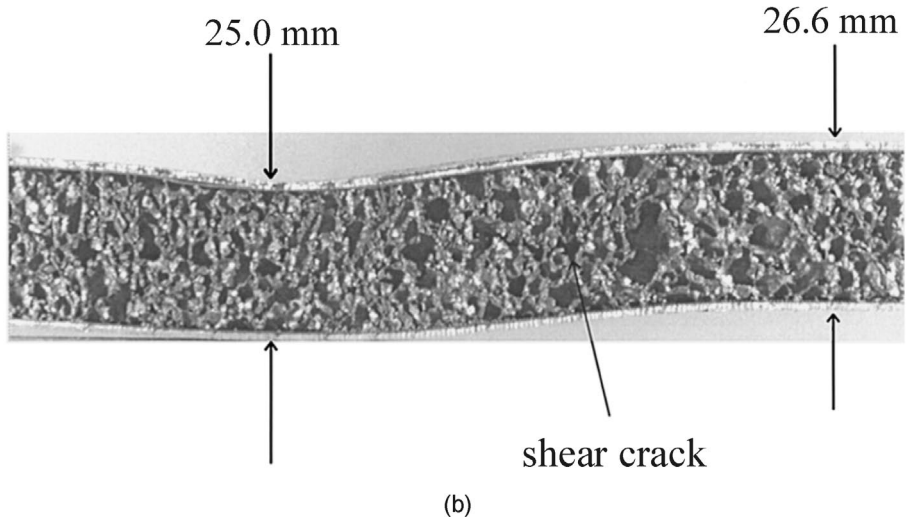

(b)

Fig. 11. (a) Load–deflection curve for sandwich beam of design 8 (test 2) showing post-peak load reduction associated with core shear failure as well as increased deflection of the upper LVDT relative to the lower LVDT, indicative of indentation failure. (b) Image of the same sandwich beam after completion of the test showing both indentation and shear failure.

shear failure are shown. The observation of both indentation and mode B core shear failure in beam designs 5, 7 and 8 suggest that the calculated transition line for these two modes is somewhat high. The transition line between core shearing by modes A and B appears to be about correct.

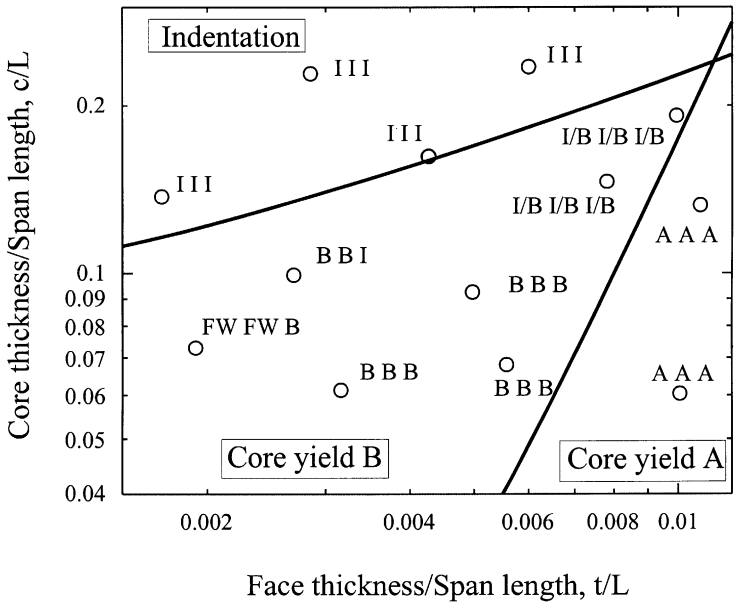

Fig. 12. Failure mode map based on the limit loads for an aluminum face, aluminum foam core sandwich beam loaded in three-point bending. The limit load failure modes of the beams tested in this study are indicated on the map.

The scatter in the measured failure loads listed in Tables 3 and 4 is due, in part, due to the variability in the foam core properties and in part, due to experimental errors such as small variations in the beam geometry or loading configuration. The density of foam specimens taken from a single sheet of foam can vary by about 10%. Since the unloading Young's modulus varies roughly with density squared and the compressive strength varies with density raised to the 3/2 power, density variations between specimens can produce a 20% variation in the unloading Young's modulus and a 15% variation in the compressive strength. Variations in the loading elastic moduli tend to be slightly higher, due to localized strain concentration effects which depend on the particular cell geometry in each specimen (Bart-Smith et al., 1998; Bastawros et al., 1998; Shepherdson, 1997).

5. Conclusions

The equations for the limit loads for indentation failure and for core shear failure by mode A or mode B give a good description of the measured peak failure loads and the dominant failure mode of aluminum foam core sandwich beams tested in three-point bending. The failure mode map can be used to identify the dominant mode of failure for a given beam design. The transition line on the failure mode map between indentation and mode B core shear failure given by the limit load equations is somewhat higher than that deduced from the results of the beam tests. The equations for initial failure, corresponding to the first deviation from linearity in the load–deflection curve, overpredict the initial failure loads, probably due to non-linearity in the stress strain curve for the foam at stresses above about one half of the compressive plateau stress.

Acknowledgements

This work was supported by the DARPA/ONR MURI Program through grant no. N00014-96-1028 for Ultralight Metal Structures. We appreciate the many helpful discussions of this topic with Professor John Hutchinson and Dr. Hilary Bart-Smith of the Division of Engineering and Applied Science of Harvard University.

References

Allen, H.G., 1969. Analysis and Design of Structural Sandwich Panels. Pergamon, New York.

American Society for Testing and Materials Standard C393-94, 1995. Test method for Flexural Properties of Flat Sandwich Constructions. Annual Book of ASTM Standards, West Conshohocken, PA.

Andrews, E.W., Gioux, G., Onck, P.R., Gibson, L.J., 2000. Size effects in ductile cellular solids Part II: Experimental results. Int. J. Mech. Sci. 43, 701–713.

Andrews, E., Sanders, W., Gibson, L.J., 1999. Compressive and tensile behaviour of aluminum foams. Mat. Sci. Engng. A270, 113–124.

Ashby, M.F., Evans, A.G., Fleck, N.A., Gibson, L.J., Hutchinson, J.W., Wadley, H.N.G., 2000. Metal foams: A Design Guide. Butterworth Heinemann, London (Chapter 10).

Bart-Smith, H., Bastawros, A.-F., Mumm, D.R., Evans, A.G., Sypeck, D.J., Wadley, H.N.G., 1998. Compressive deformation and yielding mechanisms in cellular Al alloys determined using X-ray tomography and surface strain mapping. Acta Mater. 46, 3583–3592.

Bart-Smith, H., Hutchinson, J.W., Evans, A.G., 2000. Measurement and analysis of the structural performance of cellular metal sandwich construction. Int. J. Mech. Sci., submitted for publication.

Bastawros, A.-F., Bart-Smith, H., Evans, A.G., 1998. Experimental analysis of deformation mechanisms in a closed-cell Al alloy foam. J. Mech. Phys. Solids 48, 301–322.

Chen, C., Harte, A.-M., Fleck, N.A., 2000. The plastic collapse of sandwich beams with a metallic foam core. Int. J. Mech. Sci., submitted for publication.

Deshpande, V.S., Fleck, N.A., 2000. Isotropic constitutive models for metallic foams. J. Mech. Phys. Solids 48, 1253–1283.

Gioux, G., McCormack, T.M., Gibson, L.J., 2000. Failure of aluminum foams under multiaxial loads. Int. J. Mech. Sci. 42, 1097–1117.

Miller, R.E., 2000. A continuum plasticity model for the constitutive and indentation behaviour of foamed metals. Int. J. Mech. Sci. 42, 729–754.

Onck, P.R., Andrews, E.A., Gibson, L.J., 2000. Size effects in ductile cellular solids Part I: Modelling. Int. J. Mech. Sci., 43, 681–689.

Shepherdson, E., 1997. Unpublished results.